Striking activity enhancement of gold supported on Al-Ti mixed oxide by promotion with ceria in the reduction of NO with CO

Xianwei Wang [a], Xiaoling Wu [a], Nobutaka Maeda [a,b,**], Alfons Baiker [c,*]

[a] Key Laboratory of Industrial Ecology and Environmental Engineering, School of Environmental Science and Technology, Dalian University of Technology, Dalian 116024, China
[b] Gold Catalysis Research Center, State Key Laboratory of Catalysis, Dalian Institute of Chemical Physics, Chinese Academy of Sciences, 457 Zhongshan Road, Dalian 116023, China
[c] Institute for Chemical and Bioengineering, Department of Chemistry and Applied Biosciences, ETH Zurich, Hönggerberg, HCI, CH-8093 Zurich, Switzerland

ARTICLE INFO

ABSTRACT

The promotion of an Al-Ti mixed oxide supported gold catalyst ($Au/AlTiO_x$) with ceria is shown to result in an unprecedented enhancement of its activity in the reduction of NO to N_2 with CO. The parent $Au/AlTiO_x$ catalyst was prepared by depositing 3 wt% gold on the mesoporous Al-Ti mixed oxide made by an evaporation-induced self-assembly (EISA) method using a triblock copolymer as a soft template. This parent $Au/AlTiO_x$ was impregnated with different loadings of CeO_x resulting in molar ratios of Au:Ce in the catalysts of 4:1, 2:1 and 1:1. The deposited gold particles showed a relatively broad size distribution with maxima at 8–12 nm, as evidenced by TEM. XRD and XPS analyses showed that the Al-Ti oxide support was made up of amorphous Al_2O_3-TiO_2 mixed oxide and that the Ce component was present as a mixture of Ce^{3+} (Ce_2O_3) and Ce^{4+} (CeO_2) partially covering the Au particles. The as-prepared catalysts were tested in the catalytic reduction of NO with CO in a continuous tubular microreactor at temperatures up to 300 °C. The parent $Au/AlTiO_x$ catalyst showed very low activity (8.2% NO conversion at 300 °C), whereas the ceria promoted catalyst containing a molar ratio of Au:Ce of 2:1 exhibited a dramatic enhancement of activity affording 100% NO conversion at the same conditions. The stability of this catalyst was tested in repetitive runs over 16 h time-on-stream, which showed a slight loss of activity, while 100% selectivity to N_2 was maintained. The spent catalyst could be easily regenerated reaching its original performance by heat treatment in flowing 5% O_2/He.

© 2017 Elsevier B.V. All rights reserved.

1. Introduction

The discovery of the unique catalytic activity of nano-sized Au particles has spurred extensive research on gold catalysis [1,2]. In particular, Au nanoparticles supported on metal oxides have found wide application in various important catalytic reactions, such as oxidation of CO [3] and alcohols [4,5], and hydrogenations of C=C [6] and C=O bonds [7]. In many reactions, the activity and selectivity of gold catalysts is affected by the size of the Au particles and the type of oxide support [8–14]. NO_x reduction by CO is one of the most efficient ways to eliminate CO and NO simultaneously from auto-mobile exhaust gases. Noble metals such as Rh, Pt, Pd supported on metal oxides are frequently employed for the NO—CO reaction [15–19]. Au has also been reported to catalyze the NO—CO reaction to a certain extent [12,20–23], but the application of Au catalysts has rarely been reported [10,23,24].

The use of ceria as a support material has been shown to give rise to synergistic effects and contribute to high activity of the NO—CO reaction in the presence of hydrogen because of enhanced oxygen vacancies [9,22]. Au is crucial for the formation of oxygen vacancies and reversible transformation between Ce^{4+} and Ce^{3+}. Ce-doped catalysts are considered as oxygen buffer due to the capability of storing and releasing oxygen under lean conditions [11,25]. The addition of alumina to ceria support enhances the NO conversion to some extent [9]. Bimetallic Au catalysts with cobalt, iridium and palladium are also known to improve the catalytic activity of the NO—CO reaction [26,27]. The use of TiO_2 as a support promotes the formation of isocyanate species, which is considered to be a key reaction intermediate for this reaction [28]. Although the Au-

catalyzed NO—CO reaction has been reported, most studies focus only on FT-IR investigations of NO and CO adsorptions [21,29,30], while catalytic activity for the NO—CO reaction has rarely been shown because the reaction occurs rapidly only in the presence of hydrogen [20–22]. An exception has recently been reported, where post-impregnation of Au/TiO$_2$ catalysts with FeO$_x$ showed an unprecedented enhancement of activity and selectivity in the absence of hydrogen. To our knowledge a similar strong enhancement of the catalytic performance has never been realized by the modification of oxidic supports or pre-impregnation of metal oxides [31]. Intrigued by this experience we started to explore the effect of post-impregnation of other metal oxides on supported Au catalysts.

In our search for suitable new catalytic materials for the NO reduction by CO, we prepared Au particles supported on mesoporous Al-Ti oxide, which was synthesized by an evaporation-induced self-assembly (EISA) method using a triblock copolymer as a soft template. We herein report a striking enhancement of the activity of as-prepared catalysts by post-impregnation of ceria.

2. Experimental

2.1. Catalyst preparation

Al-Ti mixed oxide (Al:Ti = 10:1) as a catalyst support was prepared using the EISA method according to the procedure reported elsewhere [32]. 10.0 g of poly(ethylene glycol)-block-poly(propylene glycol)-block-poly(ethylene glycol), (EO)$_{20}$(PO)$_{70}$(EO)$_{20}$, (Pluronic P123, Sigma-Aldrich) was dissolved in 100 ml of anhydrous ethanol (Sigma-Aldrich, ≥99.8%) together with 10 mmol of titanium (IV) isopropoxide (Sigma-Aldrich, 97%) under vigorous stirring for 4 h. Meanwhile, 90 mmol of aluminum isopropoxide (Sigma-Aldrich, 98%) was dissolved in 50 ml of anhydrous ethanol and then 16 ml of nitric acid (Sigma-Aldrich, 70% in water) was slowly added under stirring. Afterward, the two solutions were combined and stirring was continued for 5 h. The obtained slurry was transferred to an oven to evaporate the solvent at 60 °C for 48 h and then calcined at 400 °C for 4 h to form the Al-Ti mixed oxide.

The 3 wt% Au/AlTiO$_x$ catalyst was prepared by a deposition-precipitation method. An aqueous solution of Au precursor was made by dissolving 0.06 g of HAuCl$_4$·3H$_2$O (Energy chemical, 99%) powder in 100 ml of deionized water. The pH was adjusted to 7.0 by adding NH$_3$ aqueous solution (1.0 M) while the temperature was kept at 70 °C, at which the gelification occurs. 1.0 g of previously prepared Al-Ti oxide was then added and the mixture stirred for 1 h. Subsequently, the suspension was filtrated and washed by deionized water several times at room temperature. The obtained powders were dried at 60 °C in an oven overnight and then calcined at 300 °C for 1 h.

Au-CeO$_x$/AlTiO$_x$ catalysts were prepared by impregnating different amounts of the cerium precursor onto the parent Au/AlTiO$_x$ catalyst resulting in different Au/Ce molar ratios (Au:Ce = 4:1, 2:1, 1:1). The specified amounts of Au/AlTiO$_x$ and ammonium cerium(IV) nitrate (Sigma-Aldrich, 98%) were added to 50 ml of deionized water and the mixture stirred for 1 h. The suspension was then transferred to a rotary evaporator and kept under rotation at 60 °C for 1 h at atmospheric pressure. Subsequently, the suspension was cooled down to 35 °C and kept under rotation in vacuum for 1 h to evaporate the deionized water. The obtained solid was dried in an oven at 60 °C overnight and then calcined at 300 °C for 1 h. The absence of nitrate species in the calcined catalysts was confirmed by TPD (Fig. S1), which showed no evolving nitrogen oxides related to decomposition of nitrate species. The reference CeO$_x$/AlTiO$_x$ catalyst, containing the same amount of Ce as used in the preparation

of Au-Ce(2:1)/AlTiO$_x$, was synthesized in the same way using the corresponding amount of ammonium cerium(VI) nitrate. The Al-Ti mixed oxide supported catalysts with different molar ratios of Au:Ce are designated as Au, Au-Ce(4:1), Au-Ce(2:1), Au-Ce(1:1), where the cerium component existed as Ce oxides.

2.2. Catalyst characterization

BET surface area, pore volume and pore size were determined by N$_2$ adsorption at liquid N$_2$ temperature using a Quadrasorb SI instrument (Quantachrome). Before each measurement, the samples were degassed at 150 °C for 1 h to remove the adsorbed water on the surface and in the pores. The Barrett-Joyner-Halenda (BJH) analysis was applied to estimate the pore volume (V$_p$) and pore size distribution (PSD). The pore width (W$_p$) was determined at the maximum of PSD.

X-ray diffraction (XRD) measurements were performed on a PANalytical X'Pert diffractometer using Pd-filtered Cu Kα radiation at 60 kV and 55 mA.

X-ray photoelectron spectroscopy (XPS) analysis was carried out on a Thermo ESCALAB 250Xi instrument using non-monochromatized Al Kα radiation (1486.6 eV) operated at 15 kV and 10.8 mA. The powders were fixed on a sample pallet by an ultra-high vacuum resistant conductive adhesive tape in a preparation chamber. A pass energy of 50 eV was utilized to excite photoelectrons.

Transmission Electron Microscopy (TEM) images were obtained on a JEOL JEM-2100 microscope operated at 200 kV. The Au particle size range was estimated by analyzing more than 100 Au particles in the TEM images.

Temperature-programmed reduction (TPR) with H$_2$ was carried out using a Quantachrome, ChemBET Pulsar TPR/TPD instrument. 100 mg of the samples was loaded in a U-shaped quartz micro-reactor and then heated at a ramping rate of 10 °C/min in 10 vol% H$_2$ in Ar at a total flow rate of 15 ml/min. TPR signals were calibrated by injecting different amount of 10 vol% H$_2$ in Ar.

2.3. Catalytic reaction

The performance of the catalysts in the NO reduction by CO was investigated in a quartz glass fixed-bed flow reactor (inner diameter, 8 mm) loaded with 600 mg of catalysts. Prior to catalytic tests, the catalysts were pretreated with 5 vol% O$_2$ in He balance for 1 h at 300 °C. Then the reactor was cooled down to 30 °C and the reactant gas mixture (500 ppm NO, 500 ppm CO in He balance) was introduced. The catalytic activity was monitored by raising the reaction temperature at a ramping rate of 5 °C/min at a total flow rate of 300 ml/min corresponding to a gas-hourly space velocity (GHSV) of 36,000 h^{-1} (length of catalyst bed: 1 cm, catalyst bed volume: 0.5 cm^3). The NO concentration was detected by an NO—NO$_2$—NO$_x$ analyzer (Thermo Scientific, 42i-HL) at each measurement temperature after reaching a steady-state NO concentration value. The same experiments were repeated twice to ensure the reproducibility of the data. Blind test runs without catalysts showed no activity. For accurate monitoring of the N$_2$ selectivity during the stability tests, the reactant concentrations in the feed were increased (2000 ppm NO, 2000 ppm CO in He balance, 150 ml/min, 600 mg of catalyst). TCD-GC (Fili, 9750 GC) equipped with a molecular sieve 5A column was applied to analyze N$_2$ and possible byproducts.

3. Results and discussion

N$_2$ adsorption isotherms for Al-TiO$_x$, Au/AlTiO$_x$ and Au-Ce/AlTiO$_x$ catalysts with different molar ratio of Au:Ce are shown in Fig. 1. All isotherms belong to type IV with H1 hysteresis loops, which is typical for mesoporous materials. The gentle slope of the
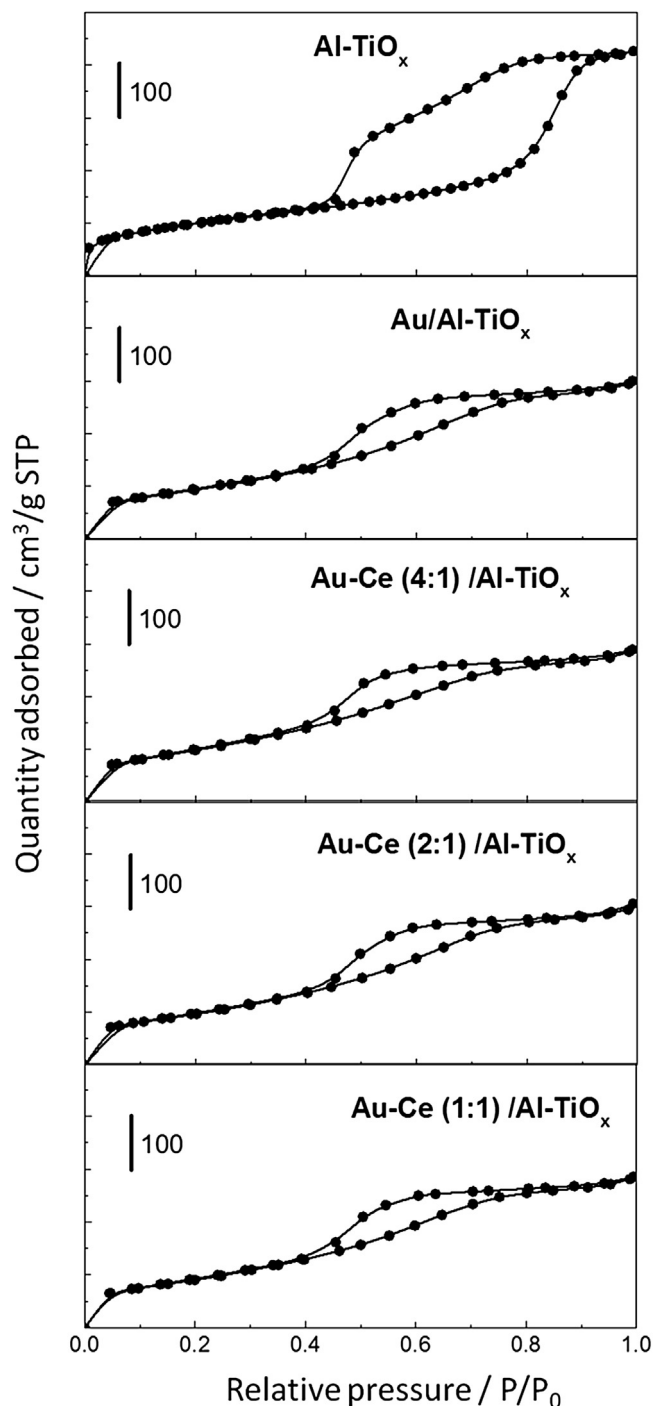
Fig. 1. Adsorption isotherms of AlTiO$_x$, Au/AlTiO$_x$ and Au-CeO$_x$/AlTiO$_x$ catalysts with different molar ratio of Au:Ce.

Table 1
Textural properties of Al-TiO$_x$, Au/Al-TiO$_x$ and Au-CeO$_x$/AlTiO$_x$ catalysts with different molar ratio of Au:Ce. S$_{BET}$: BET surface area, V$_p$: pore volume, W$_p$: pore width calculated at the maximum of PSD. Catalyst designations are given in the experimental section.

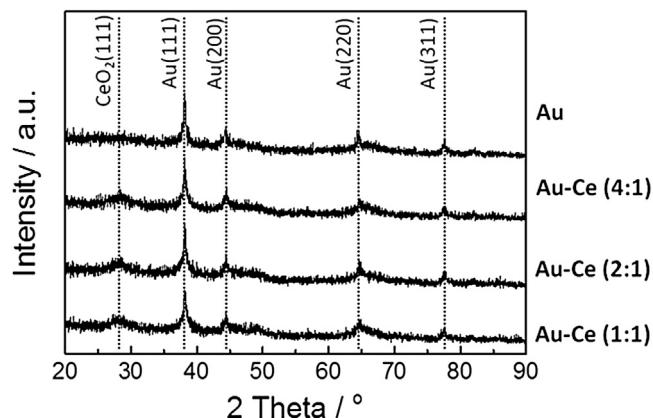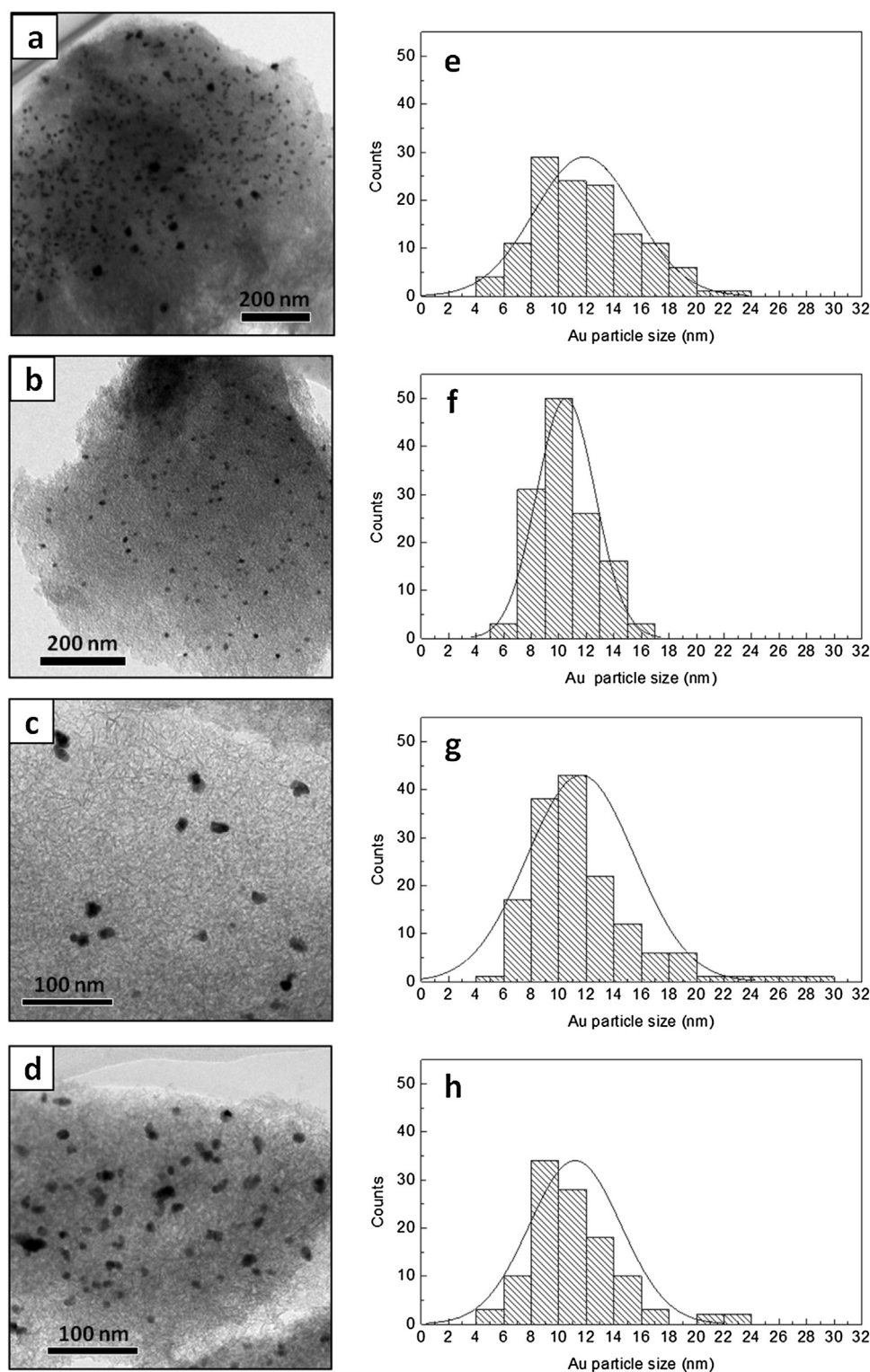| Catalyst	S$_{BET}$ (m^2/g)	V$_P$ (mL/g)	W$_P$ (nm)
AlTiO$_x$	349	0.58	12.2
Au/AlTiO$_x$	346	0.47	4.3
Au-Ce(4:1)/AlTiO$_x$	370	0.46	3.8
Au-Ce(2:1)/AlTiO$_x$	356	0.40	4.9
Au-Ce(1:1)/AlTiO$_x$	341	0.45	4.9

Fig. 2. XRD patterns of Au/AlTiO$_x$ and Au-Ce/AlTiO$_x$ catalysts with different molar ratio of Au:Ce.

capillary condensation step indicates non-uniformity and disorder of mesopores. The deposition of Au particles on the mesoporous AlTiO$_x$ resulted in a narrowing of the hysteresis loops and a slight shift of the condensation step toward lower relative pressure, indicating lower pore volume and pore diameter. BET surface areas and results from BJH analysis of the materials are summarized in Table 1.

Gold deposition on the AlTiO$_x$ support had only a small effect on the BET surface area, whereas impregnation with ceria significantly changed it. The largest surface area (370 m^2/g) was observed for the catalyst with the lowest ceria loading. The specific pore volume, and in particular the pore width decreased upon deposition of the gold

onto the AlTiO$_x$ support, while the impregnation with ceria had a less prominent effect on these properties. These results suggest that the deposition of Au particles occurred inside the disordered mesopores.

Fig. 2 shows the XRD patterns of Au/AlTiO$_x$ and Au-CeO$_x$/AlTiO$_x$ catalysts with different molar ratio of Au:Ce. All catalysts showed intense diffraction patterns of the gold face-centered cubic (fcc) phase at 2θ = 38.2°, 44.6°, 64.9° and 77.5°, corresponding to (111), (200), (220), (311) reflections, respectively (JCPDS 01-1174). Mesoporous Al$_2$O$_3$ made by the EISA method forms η-alumina [30], which shows diffraction peaks at around 2θ = 37.3°, 46.0° and 67.7° (JCPDS 1-77-396). We only confirmed small and broad peaks in these regions, suggesting the presence of amorphous alumina and trace amount of η-alumina. No diffraction patterns due to TiO$_2$ were observed in all samples, indicating that TiO$_2$ should be well-dispersed in the amorphous alumina phase. A reflection due to CeO$_2$ emerged at 2θ = 28.3° (111) after impregnation with the ceria component. However, this reflection was rather small and broad indicating that CeO$_x$ was also well-dispersed on the surface.

Fig. 3a–d shows TEM images of the catalysts, which corroborate that the mesoporous AlTi oxide is amorphous in line with the XRD results. Gold particle size distributions determined for the different catalysts based on the analysis of one hundred Au particles randomly selected from different images are shown in Fig. 3e–h. The peaks of the relatively broad distributions profiles are located at around 8–12 nm. The relatively large size of the gold particles is attributed to their propensity to agglomerate on the amorphous AlTiO$_x$ support.

XPS spectra of the Au 4f, Ti 2p, Ce 3d and Al 2p regions of the different catalysts are shown in Fig. 4. Original raw spectra without background subtraction are shown. A fitting procedure was applied for Ce 3d spectra because there were several overlapping peaks of different Ce components. The Au 4f$_{7/2}$ photoelectron peak of the Au/AlTiO$_x$ and Au-Ce(4:1)/AlTiO$_x$ located at 83.7 eV is assigned to metallic Au [33]. Further addition of Ce, as realized in Au-Ce(2:1)/AlTiO$_x$ and Au-Ce (1:1)/Al-TiO$_x$, led to a negative shift

Fig. 3. TEM images and size distribution profiles of Au particles of (a, e) Au/AlTiO$_x$, (b, f) Au-Ce(4:1)/AlTiO$_x$, (c, g) Au-Ce(2:1)/AlTiO$_x$ and (d, h) Au-Ce(1:1)/AlTiO$_x$.

of the Au 4f$_{7/2}$ signal to 83.5 eV. The CeO$_x$ addition has been proposed to promote the electron transfer from metal oxides (CeO$_x$, TiO$_2$, Al$_2$O$_3$) to the Au particles [34]. In general, the adsorption of gaseous molecules on Au is rather weak, but the resulting negatively charged Au particles are reported to enhance the affinity of molecules to Au and thus to enrich active gas molecules on the surface [35]. The Ti 2p and Al 2p peaks are typical for TiO$_2$ (Ti^{4+}) and Al$_2$O$_3$ (Al^{3+}), and no signal due to Ti^{3+} was observed [36]. These

signals showed no obvious change in the binding energy originating from the addition of CeO$_x$. The Ce 3d spectra are composed of two multiplets (v and u). They correspond to the spin-orbit splitting 3d$_{5/2}$ and 3d$_{3/2}$. The peaks of U^{III}, U^{II}, U, V^{III}, V^{II} and V located at 916.7 eV, 907.5 eV, 901.0 eV, 898.6 eV, 889.3 eV and 882.4 eV, respectively, are characteristic of tetravalent Ce^{4+} (CeO$_2$) in the CeO$_x$. The peaks of U^{I} and V^{I} located at 903.8 eV and 885.6 eV originate from Ce^{3+}, as present in Ce$_2$O$_3$ [37,38], indicating that
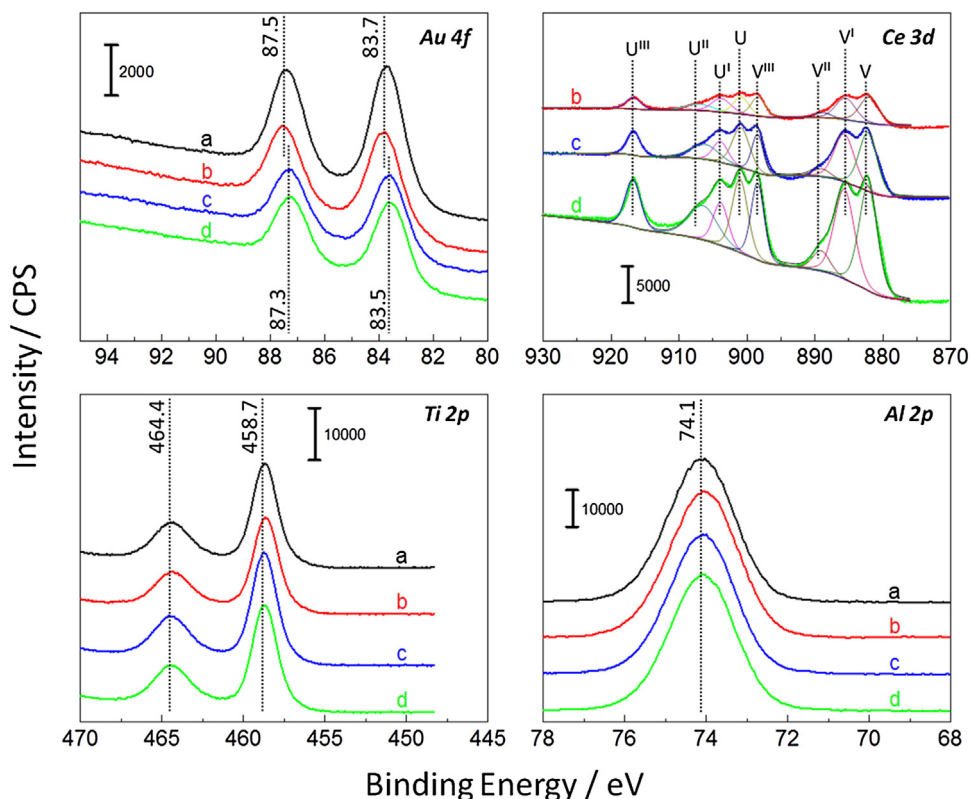
Fig. 4. XPS analyses of Au 4f, Ce 3d, Ti 2p and Al 2p regions for (a) Au/AlTiO$_x$, (b) Au-Ce(4:1)/AlTiO$_x$, (c) Au-Ce(2:1)/AlTiO$_x$ and (d) Au-Ce(1:1)/AlTiO$_x$ catalysts.

Table 2
XPS analyses of Au/AlTiO$_x$ and Au-CeO$_x$/AlTiO$_x$ catalysts with different molar ratio of Au:Ce.

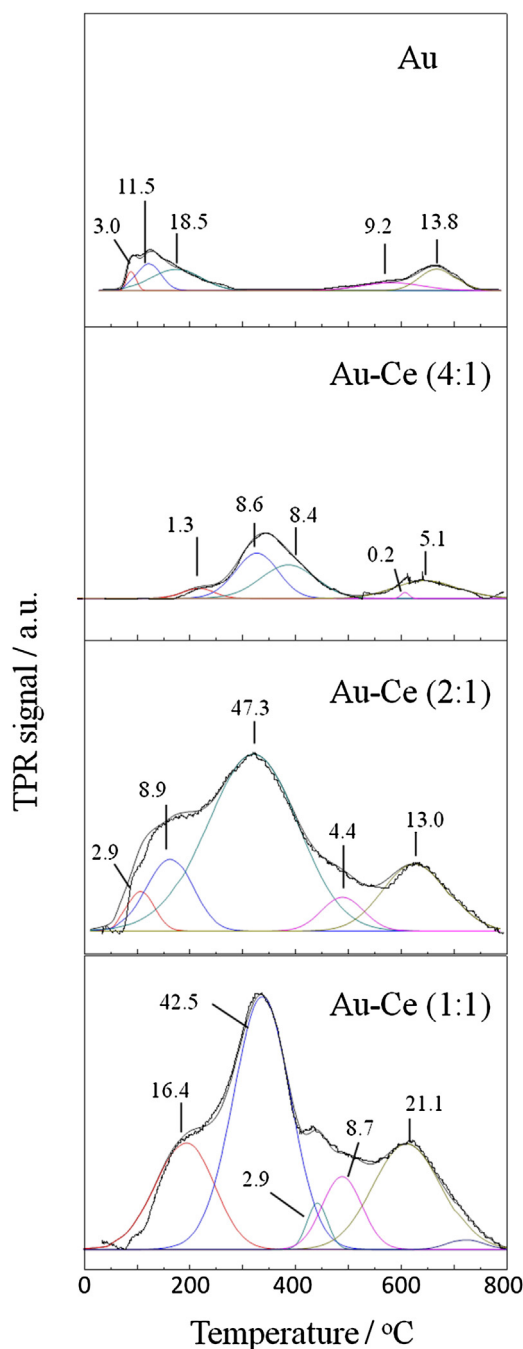| Catalyst	XPS		
	BE of Au4f$_{7/2}$ (eV)	Au/(Ce^{3+}+ Ce^{4+})	Ce^{3+}/(Ce^{3+}+ Ce^{4+})
Au/AlTiO$_x$	83.7	–	–
Au-Ce(4:1)/AlTiO$_x$	83.7	1.67	0.45
Au-Ce(2:1)/AlTiO$_x$	83.5	0.61	0.46
Au-Ce(1:1)/AlTiO$_x$	83.5	0.35	0.40

a mixture of Ce^{3+} and Ce^{4+} oxidation states existed on the surface of the catalysts. The Ce oxides are therefore denoted as CeO$_x$ (x = 1.5–2). As shown in Table 2, the concentration of Ce^{3+} slightly decreased for Au-Ce(1:1)/AlTiO$_x$. On the other hand, the addition of Ce had a considerable impact on the Au/Ce ratio: 1.67 for Au-Ce (4:1)/AlTiO$_x$ and 0.35 for Au-Ce (1:1)/AlTiO$_x$, respectively.

Fig. 5 shows H$_2$-TPR profiles of the different catalysts. The reduction peak centered at around 350 °C increased with the amount of CeO$_x$ added. This peak originates from the reaction of the surface oxygen of CeO$_2$, which can be reduced at lower temperature compared to bulk CeO$_2$ [39]. The broad peak at around 100–220 °C can be assigned to the reduction of Ce^{4+} capping Au nanoparticles [39–41]. The TPR results are in good agreement with the XPS analyses, which indicate the presence of Ce^{4+} as CeO$_2$.

Fig. 6 shows the NO conversion during the reduction of NO by CO. The selectivity to N$_2$ is not shown because at the conditions used the concentration of N$_2$ was fairly low (close to the detection limit of TCD-GC), therefore the data were not reliable. Information on the selectivity was thus gained at conditions more suitable for accurate analysis by TCD-GC (vide infra). As expected, Au/AlTiO$_x$ exhibited very low activity in the whole temperature range (8.2% NO conversion at 300 °C) probably because of the relatively large Au particle size. The addition of CeO$_x$ strongly enhanced the catalytic
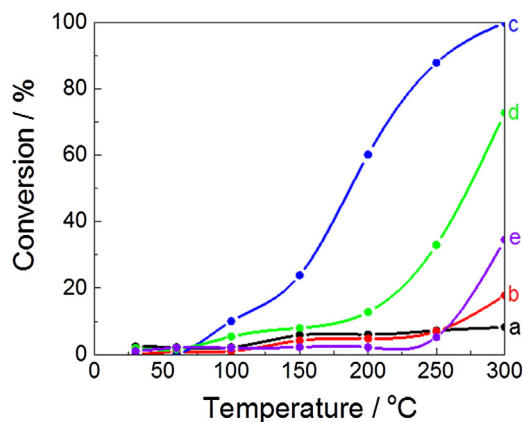
activity compared to the parent Au/AlTiO$_x$ catalyst. The activity of Au-Ce(4:1)/AlTiO$_x$ was only moderately higher at 300 °C (17.8% NO conversion) due to the low ceria content, but further addition of CeO$_x$ dramatically increased the activity. Au-Ce(2:1)/AlTiO$_x$ showed 87.8% NO conversion at 250 °C and 100% at 300 °C, respectively. A similarly prepared CeO$_x$/AlTiO$_x$ reference catalyst with the same content of ceria showed poor activity up to 250 °C, but its NO conversion increased to 34.6% at 300 °C. However, the conversion of Au-Ce(2:1)/AlTiO$_x$ at 300 °C (100%) was still much higher than the sum (ca. 43%) of the expected contributions from the individual catalysts (Au/AlTiO$_x$: 8.2%, CeO$_x$/AlTiO$_x$: 34.6%). To the best of our knowledge, such striking enhancement of the activity of the Au-catalyzed NO—CO reaction by CeO$_x$ promotion has not been reported so far, particularly not in the absence of hydrogen. However, further CeO$_x$ addition, as represented by Au-Ce(1:1)/AlTiO$_x$, deteriorated the activity probably because of high coverage of Ce oxides on the Au particles, as evident from the XPS analyses (see Au/(Ce^{3+} + Ce^{4+}) ratio in Table 2).

Fig. 7 shows a stability test of the best performing Au-Ce(2:1)/AlTiO$_x$ catalyst. To detect any possible byproducts and confirm the high selectivity to N$_2$, the reaction conditions were changed to 2000 ppm NO, 2000 ppm CO, He balance, total flow rate: 150 ml/min, catalyst load: 600 mg, reaction temperature: 300 °C. The four times higher inlet concentration of reactants led to lower NO conversion than in the tests shown in Fig. 6. The lower NO conversion with higher feed concentrations of reactants is attributed to a lowering of the reaction rate caused by higher coverage of CO on the Au surface, which suppresses the NO adsorption and dissociation [31]. In addition with higher feed concentrations more NO molecules have to be reduced for achieving a specific conversion X (X = n$_o$-n/n$_o$, where n$_o$ and n are the number of NO molecules at reactor inlet and outlet, respectively). After the 16 h test, the spent catalyst was regenerated by flowing 5 vol% O$_2$/He at 300 °C for 1 h through the catalyst bed and then used again in a second and a third
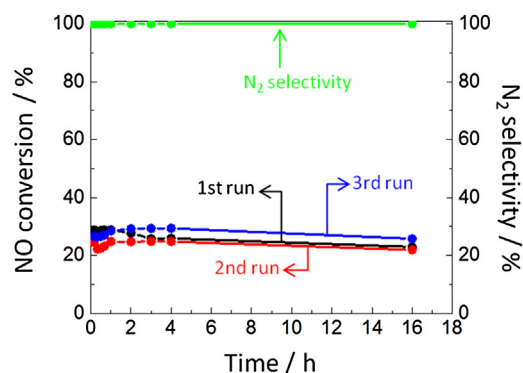
Fig. 5. H$_2$-TPR profiles of Au/AlTiO$_x$ and Au-Ce/AlTiO$_x$ catalysts with different molar ratio of Au:Ce. Conditions: catalyst weight: 100 mg, gas mixture: 10 Vol% H$_2$ in Ar balance, ramping rate: 10 °C/min, total flow rate: 15 ml/min. Numbers assigned to profiles represent the amount of hydrogen consumed (μmol/g-catalyst) in the corresponding deconvoluted signals.

Fig. 6. NO-conversion of (a) Au/AlTiO$_x$, (b) Au-Ce(4:1)/AlTiO$_x$, (c) Au-Ce(2:1)/AlTiO$_x$, (d) Au-Ce(1:1)/AlTiO$_x$ and (e) Ce/AlTiO$_x$ catalysts; gas mixture: 500 ppm NO, 500 ppm CO, He balance, total flow rate: 300 ml/min, reaction temperature: 30–300 °C.

Fig. 7. Stability and recyclability test of Au-Ce(2:1)/AlTiO$_x$. Conditions: gas mixture 2000 ppm NO, 2000 ppm CO, He balance, total flow rate: 150 ml/min, catalyst loaded: 600 mg, reaction temperature: 300 °C.

run. The NO-conversion slightly changed for each run, but stayed at similar level. No byproducts were detected confirming that the N$_2$ selectivity was at 100% throughout every run under these conditions. The reduction of NO by CO proceeds via the following steps [42,43]:

$$NO + CO \rightarrow 1/2\,N_2 + CO_2 \tag{1}$$

$$2\,NO + CO \rightarrow N_2O + CO_2 \tag{2}$$

$$N_2O + CO \rightarrow N_2 + CO_2 \tag{3}$$

The formation of CO$_2$ occurs by a direct path (reaction 1) and a sequential path (reactions 2 and 3). Since the N$_2$ selectivity was 100%, we infer that reaction 1 (direct NO—CO reaction) occurred as a main reaction pathway or reaction 3 (N$_2$O—CO reaction) took place rapidly.

Attempts to gain further information about the activity enhancement by in situ diffuse reflectance IR Fourier transform spectroscopy (DRIFTS) failed due to low amplitude (less than 300) at the MCT detector caused by intense IR absorption of the catalysts. In general, large Au particles (>10 nm) are believed to be quite inactive for catalytic reactions, in line with our data for Au/AlTiO$_x$. However, the simple modification of Au particles by post-impregnation of Ce oxides, shown in this study, can trigger the activity and leads to a potentially efficient catalytic material for the NO reduction by CO. Although, the exact role of CeO$_x$ remains unclear, there exists a study, where it is reported that high surface concentration of Ce^{3+} species (ca. 15–28%) correlates with high catalytic activity for the NO reduction by CO and H$_2$ due to efficient redox reactions [22]. Since our catalysts contained a high fraction of Ce^{3+} (ca. 46%) as shown in Table 2, the activity enhancement generated by CeO$_x$ may be speculated to result from the unique redox property of the CeO$_x$ promoter. However, the high concentration of Ce^{3+} alone cannot account for the very high NO conversion of Au-Ce(2:1)/AlTiO$_x$. The Au/Ce ratio in the near-surface region as probed by XPS (Table 2) is also crucial. This ratio ranged from 1.67 to 0.35, depending on the amount of CeO$_x$ added. Maximizing the promotional effect of CeO$_x$ requires proper balancing of the Au/Ce surface ratio. The promotional effect decreases at too high CeOx loading

probably due to blocking of the Au surface. This explains why the Au-Ce(2:1)/AlTiO$_x$ with a surface Au/Ce ratio of 0.61 shows highest activity. The observed beneficial synergy between Au and CeO$_x$ may be further enhanced by maximizing the Au-CeO$_x$ interfacial contact, as e.g. by lowering the Au particle size.

4. Conclusions

Amorphous, mesoporous Al-Ti mixed oxide with high surface area, prepared by means of the evaporation-induced self-assembly (EISA) method was employed as a support for gold-based catalysts. XRD analysis indicated that both Ti and Ce oxides were amorphous or well-dispersed in the Al$_2$O$_3$ matrix. The Au particles deposited on the AlTiO$_x$ support showed poor catalytic activity in the reduction of NO with CO even at relatively high temperature (300 °C). However, the promotion of this catalyst by post-impregnation of a suitable amount of CeO$_x$ lead to a very strong enhancement of the activity showing 100% NO conversion at the same conditions. The added CeO$_x$ partially covered the Au particles and existed as Ce^{3+} (Ce$_2$O$_3$) and Ce^{4+} (CeO$_2$) species, as evidenced by XPS. The unprecedented enhancement of the activity upon CeO$_x$ promotion was strongly dependent on the CeO$_x$ loading. Catalysts with a molar ratio of Au:Ce of 2:1 showed best catalytic performance, while lower and higher CeO$_x$ loading, as realized in Au-Ce(1:1)/AlTiO$_x$ and Au-Ce(4:1)/Al-TiO$_x$, were significantly less active, indicating that there exists a sensitive balance between the promotional effect of Ce oxides and the deactivation by covering the Au surface. Maximizing the interfacial contact between Au and CeO$_x$ seems a promising strategy to further improve the catalytic behavior of the Au-based catalysts for the reduction of NO with CO.

Acknowledgements

Appendix A. Supplementary data

Supplementary data associated with this article can be found, in the online version, at http://dx.doi.org/10.1016/j.apcatb.2017.02.070.

References

[1] M. Haruta, T. Kobayashi, H. Sano, N. Yamada, Chem. Lett. 16 (1987) 405–408.
[2] G.J. Hutchings, J. Catal. 96 (1985) 292–295.
[3] M. Haruta, Gold Bull. 37 (2004) 27–36.
[4] P. Haider, B. Kimmerle, F. Krumeich, W. Kleist, J.-D. Grunwaldt, A. Baiker, Catal. Lett. 125 (2008) 169–176.
[5] B. Kimmerle, J.-D. Grunwaldt, A. Baiker, Top. Catal. 44 (2007) 285–292.
[6] M. Stratakis, H. Garcia, Chem. Rev. 112 (2012) 4469–4506.
[7] Y. Zhang, X. Cui, F. Shi, Y. Deng, Chem. Rev. 112 (2012) 2467–2505.
[8] L. Ilieva, G. Pantaleo, I. Ivanov, R. Zanella, A.M. Venezia, D. Andreeva, Int. J. Hydrogen Energy 34 (2009) 6505–6515.
[9] L. Ilieva, G. Pantaleo, I. Ivanov, A.M. Venezia, D. Andreeva, Appl. Catal. B-Environ. 65 (2006) 101–109.
[10] C. Ge, L. Liu, Z. Liu, X. Yao, Y. Cao, C. Tang, F. Gao, L. Dong, Catal. Commun. 51 (2014) 95–99.
[11] Y. Kuwauchi, H. Yoshida, T. Akita, M. Haruta, S. Takeda, Angew. Chem. Int. Ed. 51 (2012) 7729–7733.
[12] L. Ilieva, G. Pantaleo, N. Velinov, T. Tabakova, P. Petrova, I. Ivanov, G. Avdeev, D. Paneva, A.M. Venezia, Appl. Catal. B-Environ. 174–175 (2015) 176–184.
[13] A. Ueda, M. Haruta, Appl. Catal. B-Environ. 18 (1998) 115–121.
[14] M. Haruta, Catal. Today 36 (1997) 153–166.
[15] T. Uchiyama, R. Karita, M. Nishibori, H. Einaga, Y. Teraoka, Catal. Today 251 (2015) 7–13.
[16] V. Ferrer, D. Finol, R. Solano, A. Moronta, M. Ramos, J. Environ. Sci. 27 (2015) 87–96.
[17] P. Xiao, R.C. Davis, X. Ouyang, J. Li, A. Thomas, S.L. Scott, J. Zhu, Catal. Commun. 50 (2014) 69–72.
[18] M. Li, X. Wu, Y. Cao, S. Liu, D. Weng, R. Ran, J. Colloid Interface Sci. 408 (2013) 157–163.
[19] E.R. Essinger-Hileman, D. DeCicco, J.F. Bondi, R.E. Schaak, J. Mater. Chem. 21 (2011) 11599–11604.
[20] L. Ilieva, G. Pantaleo, J.W. Sobczak, I. Ivanov, A.M. Venezia, D. Andreeva, Appl. Catal. B-Environ. 76 (2007) 107–114.
[21] L. Ilieva, G. Pantaleo, I. Ivanov, R. Nedyalkova, A.M. Venezia, D. Andreeva, Catal. Today 139 (2008) 168–173.
[22] L. Ilieva, G. Pantaleo, R. Nedyalkova, J.W. Sobczak, W. Lisowski, M. Kantcheva, A.M. Venezia, D. Andreeva, Appl. Catal. B-Environ. 90 (2009) 286–294.
[23] N. Liu, X. Chen, J. Zhang, J.W. Schwank, Catal. Today 258 (Pt. 1) (2015) 139–147.
[24] G.R. Garda, N.J. Castellani, Appl. Catal. A-Gen. 494 (2015) 48–56.
[25] M. Kantcheva, M. Milanova, S. Mametsheripov, Catal. Today 191 (2012) 12–19.
[26] H.U. Shin, D. Lolla, Z. Nikolov, G.G. Chase, J. Ind. Eng. Chem. 33 (2016) 91–98.
[27] Y.-J. Song, Y.M. Lopez-De Jesus, P.T. Fanson, C.T. Williams, Appl. Catal. B-Environ. 154 (2014) 62–72.
[28] F. Solymosi, T. Bánsági, T.S. Zakar, Phys. Chem. Chem. Phys. 5 (2003) 4724–4730.
[29] M. Centeno, C. Portales, I. Carrizosa, J. Odriozola, Catal. Lett. 102 (2005) 289–297.
[30] M. Kantcheva, M. Milanova, I. Avramova, S. Mametsheripov, Catal. Today 187 (2012) 39–47.
[31] X. Wang, N. Maeda, A. Baiker, ACS Catal. 6 (2016) 7898–7906.
[32] S.M. Morris, P.F. Fulvio, M. Jaroniec, J. Am. Chem. Soc. 130 (2008) 15210–15216.
[33] M.P. Casaletto, A. Longo, A. Martorana, A. Prestianni, A.M. Venezia, Surf. Interface Anal. 38 (2006) 215–218.
[34] J. García-Serrano, A.G. Galindo, U. Pal, Sol. Energy Mater. Sol. Cells 82 (2004) 291–298.
[35] D. Horváth, L. Toth, L. Guczi, Catal. Lett. 67 (2000) 117–128.
[36] N. Kruse, S. Chenakin, Appl. Catal. A: Gen. 391 (2011) 367–376.
[37] W. Zhu, S. Xiao, D. Zhang, P. Liu, H. Zhou, W. Dai, F. Liu, H. Li, Langmuir 31 (2015) 10822–10830.
[38] E. Bêche, P. Charvin, D. Perarnau, S. Abanades, G. Flamant, Surf. Int. Anal. 40 (2008) 264–267.
[39] Y. Liu, B. Liu, Q. Wang, Y. Liu, C. Li, W. Hu, P. Jing, W. Zhao, J. Zhang, RSC Adv. 4 (2014) 5975–5985.
[40] A. Sandoval, A. Gómez-Cortés, R. Zanella, G. Díaz, J.M. Saniger, J. Mol. Catal. A: Chem. 278 (2007) 200–208.
[41] D. Andreeva, V. Idakiev, T. Tabakova, L. Ilieva, P. Falaras, A. Bourlinos, A. Travlos, Catal. Today 72 (2002) 51–57.
[42] J.H. Holles, R.J. Davis, T.M. Murray, J.M. Howe, J. Catal. 195 (2000) 193–206.
[43] J.H. Holles, M.A. Switzer, R.J. Davis, J. Catal. 190 (2000) 247–260.